Closed-loop Superconducting Materials Discovery

Elizabeth A. Pogue[1*†], Alexander New[1†], Kyle McElroy[1], Nam Q. Le[1], Michael J. Pekala[1], Ian McCue[1], Eddie Gienger[1], Janna Domenico[1], Elizabeth Hedrick[2], Tyrel M. McQueen[2,3,4*], Brandon Wilfong[3,4], Christine D. Piatko[1], Christopher R. Ratto[1], Andrew Lennon[1], Christine Chung[1], Timothy Montalbano[1], Gregory Bassen[3,4] and Christopher D. Stiles[1*]

[1*]Research and Exploratory Development Department, Johns Hopkins University Applied Physics Laboratory, 11100 Johns Hopkins Road, Laurel, 20723, Maryland, United States of America.

[2]Department of Materials Science and Engineering, Johns Hopkins University, 3400 N. Charles Street, Baltimore, 21218, Maryland, United States of America.

[3]Department of Chemistry, Johns Hopkins University, 3400 N. Charles Street, Baltimore, 21218, Maryland, United States of America.

[4]Institute for Quantum Matter, William H. Miller III Department of Physics and Astronomy, Johns Hopkins University, 3400 N. Charles Street, Baltimore, 21218, Maryland, United States of America.

[5]Department of Materials Science and Engineering, Northwestern University, 2220 Campus Drive, Evanston, 60208, Illinois, United States of America.

*Corresponding author(s). E-mail(s): Lisa.Pogue@jhuapl.edu; mcqueen@jhu.edu; Christopher.Stiles@jhuapl.edu;

Contributing authors: Alex.New@jhuapl.edu;
Kyle.McElroy@jhuapl.edu; Nam.Q.Le@jhuapl.edu;
Michael.Pekala@jhuapl.edu; Ian.McCue@northwestern.edu;
Eddie.Gienger@jhuapl.edu; Janna.Domenico@jhuapl.edu;
ehedric4@jhu.edu; bwilfon3@jhu.edu;
Christine.Piatko@jhuapl.edu; Christopher.Ratto@jhuapl.edu;
Andrew.Lennon@jhuapl.edu; Christine.Chung@jhuapl.edu;
Timothy.Montalbano@jhuapl.edu; gbassen1@jhu.edu;
†These authors contributed equally to this work.

Keywords: machine learning, superconductivity, discovery

Supplementary Methods

Here we go into more detail about the approach used in RooSt [1] to map a material composition to a predicted property. The composition is encoded as a fully-connected graph, where each node i corresponds to an atomic species found in that composition. Each species i has an initial representation vector h_i^0 specified by the user (e.g., a one-hot encoding of species type), and the fraction w_i of the composition it makes up (e.g., for $Zr_3Fe_4Sn_4$, $w_{Zr} = 3/15$). A series of $t = 0, \ldots, T-1$ message-passing updates iteratively update each species representation vector to h_i^{t+1} as follows:

$$e_{i,j}^{t,m} = f^{t,m}(h_i^t, h_j^t) \tag{1}$$

$$a_{i,j}^{t,m} = \frac{w_j \exp(e_{i,j}^{t,m})}{\sum_k w_k \exp(e_{i,k}^{t,m})} \tag{2}$$

$$h_i^{t+1} = h_i^t + \sum_{m,j} a_{i,j}^{t,m} g^{t,m}(h_i^t, h_j^t), \tag{3}$$

where i and j are species indices, $f^{t,m}$ and $g^{t,m}$ are multi-layer perceptrons, $a_{i,j}^{t,m}$ are soft attention coefficients computed with a weighted softmax, and

Supplementary Table 1 Precursor List for Experimental Runs

Element or Compound	Source	Form	Purity
Mg	Alfa Aesar	turnings, 3.2 mm wide	99.8%
$MgSi_2$	Beantown Chemical	powder	99.5%
Ca	Alfa Aesar	granules, -16 mesh	99.5 %
Sc	Alfa Aesar	pieces	99.9 %
Ti	Alfa Aesar	foil, 0.25 mm	99.5 %
Zr	Strem	foil	99.8%
Hf	Alfa Aesar	foil, 0.025 mm	99.5 %
V	Alfa Aesar	foil, 0.127 mm	99.8 %
	Alfa Aesar	wire, 1.5 mm	99.8 %
Nb	Alfa Aesar	foil, 0.3 mm	99.8 %
	Alfa Aesar	foil, 0.025 mm	99.8 %
	Strem	foil	99.8 %
Ta	Alfa Aesar	foil, 0.025 mm	99.95 %
	Beantown Chemical	foil, 0.025 mm	99.95 %
Mo	Beantown Chemical	foil, 0.025 mm	99.95 %
W	Alfa Aesar	wire, 0.75 mm diameter	99.95 %
Mn	Beantown Chemical	pieces	99.95 %
Fe	Goodfellow	foil	99.8 %
Co	Alfa Aesar	pieces	99.9+ %
Co	Aldrich	pieces	99.5 %
Ni	Alfa Aesar	foil	99+%
	Alfa Aesar	-300 mesh	99.8%
Cu	Strem	foil	99.9 %
	Alfa Aesar	powder, -325 mesh	99%
	Alfa Aesar	shot, 4-6 mm, Pufratronic	99.999%
Ag	Alfa Aesar	wire	99.9 %
Zn	Alfa Aesar	ingot	99.99 %
B	Alfa Aesar	powder, -325 mesh	98 %
Al	Beantown Chemical	wire, 1.0 mm diameter	99.999 %
Ga	NOAH Tech	chunks	99.99 %
In	Alfa Aesar	shot, 4 mm tear drop	99.99 %
C	Alfa Aesar	graphite rod, 6.15 mm diameter	99.9995%
Si	Alfa Aesar	lump	99.999+%
Ge	Beantown Chemical	pieces, 3-9 mm	99.999%
Sn	Beantown Chemical	shot (8-20 mesh)	99.5 %
	Beantown Chemical	granules	99.9 %
Pb	Alfa Aesar	pieces	99.999 %
P	Sigma Aldrich	red, powder	97+%
Bi	Alfa Aesar	needles, 1-5 cm, 1.5 mm diameter	99.99%
S	Alfa Aesar	powder, Puratronic	99.999%
Yb	Alfa Aesar	pieces, sublimed	99.9 %

the index m denotes separate "attention heads" that stabilize training and improve model expressivity.

The final species representation vectors h_i^T are gathered into a material-level representation vector h after a final soft-attention operation and then fed through a final MLP f^y to yield a predicted property $\hat{y}$:

$$e_i^{T,m} = f^{T,m}(h_i^T) \tag{4}$$

$$a_i^{T,m} = \frac{w_i \exp(e_i^{T,m})}{\sum_j w_j \exp(e_j^{T,m})} \tag{5}$$

$$h = \sum_{m,i} a_i^{T,m} g^{T,m}(h_i^T) \tag{6}$$

$$\hat{y} = f^y(h) \tag{7}$$

Note that pure (unary) elemental materials are not amenable to this representation and cannot be ingested by a RooSt model.

All of the model's weights for the message-passing and prediction mechanisms (i.e., each $f^{t,m}$ and $g^{t,m}$, and f^y, are trained in an end-to-end manner using a cross-entropy loss.

For arc melting, more volatile components were wrapped in metallic foils of less-volatile components and melted with a full-scale current of ∼50-100 A with ∼0.7 atm argon present in the vacuum chamber. Zirconium metal, which reacts quickly with oxygen, was first melted in the chamber after it was filled with argon to remove any remaining oxygen before the samples were melted. Samples were melted 2-3 times, flipped, and then melted 2-3 times. If evidence of a superconducting transition was observed, homogenizing heat treatments were performed at temperatures that depended on the chemistry of the sample (generally near 1000 °C for times ranging from overnight to several days).

For metals containing magnesium or calcium, due to their tendency to vaporize, arc melting was not feasible. $CaIn_6Cu_6$, $Ca(Al_2Cu)_4$, $Ca(AgGe)_2$, Ca_2Zn_3Ag, $Ca_3(Cu_2Sn)_4$, and $CaCu_9Sn_4$ were made by wrapping samples in tantalum foil (to minimize reactions with the quartz ampoule) and sealing them in evacuated quartz ampoules. The samples were then heated to 700 °C for 2 h and the furnace was turned off and allowed to naturally cool. The same was done for $Ca_3(Cu_2Sn)_4$, $CaCu_9Sn_4$, $Ca(CuSi_{0.33}Sn_{0.33}Ge_{0.33})_2$, Ca_2Zn_3Ag, and $Ca(AgGe)_2$ except the anneal was performed at 900 °C. Vaporization of

magnesium in ampoules was more of an issue for the Mg-containing samples compared to calcium vaporization in the Ca-containing samples. Samples with nominal MgCuSn, and MgCuBi compositions were similarly wrapped in tantalum foil and sealed in evacuated quartz ampoules. The samples were then heated in a box furnace to 900 °C for 2 h. The furnace was then turned off and the samples allowed to cool to room-temperature. Since tantalum foil has a T_c of 4 K, it was important to separate the samples from the foil before measuring AC susceptibility. This was much more difficult for some of the Mg-containing samples so we also attempted to make MgCuSn and Mg_2Cu_3Si wrapped in molybdenum foil using the same procedures. These samples tended to react with the molybdenum foil and, therefore, did not form the targeted phases.

Supplementary Discussion

We synthesized many binaries and did not see evidence of superconductivity above 2 K unrelated to indium. A small, very broad diamagnetic signal was observed in a $ZrIn_3$ sample that went away upon annealing. The intensity of the superconducting signal was largest for compositions near "$ZrNiIn_4$". XRD showed that these specimens were not phase pure, and contained compounds not known to superconduct above 4 K.

Magnetic susceptibility measurements for $ZrNi_2In$ reported in 1999 showed no evidence of a superconducting signal [2]. However, in 2004, members of the same group presented at E-MRS that $ZrNi_2In$ superconducts with a T_c of 9 K [3], suggesting there is a 9 K superconductor somewhere in this ternary phase diagram (There is no archival paper that we could locate and no data is readily available.) The abstract for the E-MRS talk did not make note of the indium-rich conditions that we observed seem required. The isostructural compounds $ZrNi_2Ga$ and $ZrNi_2Al$ superconduct with a T_c of 2.9 K and 1.38 K,

respectively [4, 5]. Their superconductivity has been attributed to a Van Hove singularity at the L point near the Fermi level that should also be present in $ZrNi_2In$ [4, 6]. Nearly phase-pure $ZrNi_2In$ had a weak signal compared to more In-rich compositions, indicating that the superconducting phase observed here is not due to stoichiometric $ZrNi_2In$.

One alternate explanation of the ∼9 K signal that we investigated in detail was the possibility of ZrN traces contributing to the signal. Gold-colored flecks were observed in some of the strongly superconducting arc melted samples and cubic ZrN is the only known gold-colored phase that had any chance of being present. Cubic ZrN has a T_c of 9.8-10.0 K, so an air leak might explain the observed ∼9 K T_c [7]. Samples shown by XRD to definitively contain ZrN (Zr_2InNi and ZrNi, melted under nitrogen) showed a T_c below 6 K. No superconducting transition was observed in ZrNi samples melted under argon, demonstrating that indium is necessary for the ∼9 K T_c.

The strongest signal that we achieved in arc melted samples came from a sample melted under argon and annealed for 5.5 days at 1000 °C. This anneal allowed indium to vapor transport away from the bulk of the sample. Parts of the sample with a shiny gray and gold appearance had a comparatively strong superconducting signal (Figure 3a).

Supplementary Figures and Tables

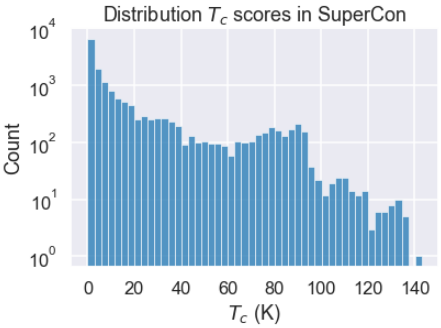

Supplementary Figure 1 Distribution of raw T_c values in the version of SuperCon used as training data. The data are long-tailed with a small number of high-T_c outliers.

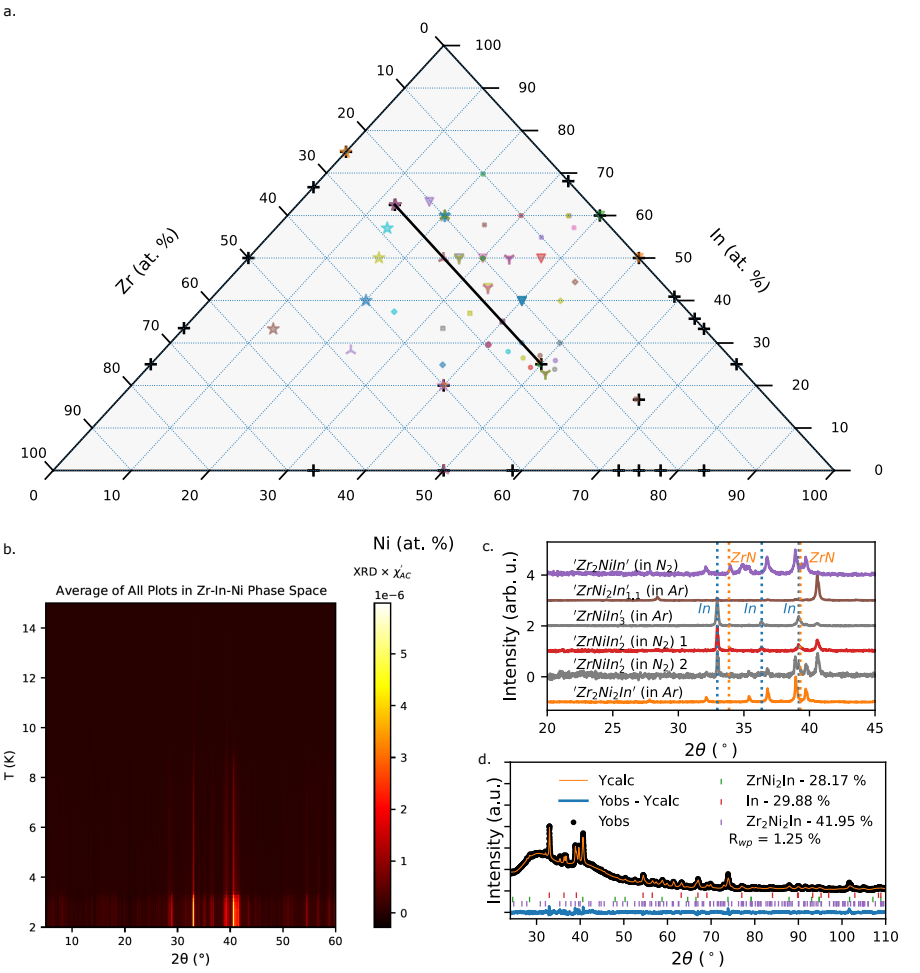

Supplementary Figure 2 (a) All samples within the Zr-In-Ni phase diagram that were made, including several binary alloys. (b) shows a heat map averaged over all the samples in the system where the color equals the normalized XRD intensity multiplied by χ'_{AC} ($color = -\chi'_{AC} \times Intensity_{XRD}$). Indium is consistently present in samples with strong superconducting signals below 3.4 K but cannot explain the ∼9 K transition that is consistently observed. (c) and (d) show how XRD was used to identify the phases present in samples with and without strong superconducting signals. Indium diffraction peaks were used as an internal standard to correct for sample height variations since In-rich samples were extremely malleable and could not be made into a powder. The nominally $ZrNi_2In_{1.1}$ sample contained only indium and $ZrNi_2In$. The nominally Zr_2Ni_2In sample was primarily Zr_2Ni_2In. Rietveld refinements of samples containing a strong superconducting signal (d) showed indium, $ZrNi_2In$, and Zr_2Ni_2In present. Our Zr_2Ni_2In sample did not superconduct, implying that $ZrNi_2In$ does superconduct under certain indium-rich conditions. To rule out ZrN impurities as the superconducting phase, a number of samples were melted in nitrogen. Samples intentionally made with the largest amount of ZrN present based on XRD had a T_c below 6 K and, therefore, ZrN impurities would not explain the ∼9 K transition.

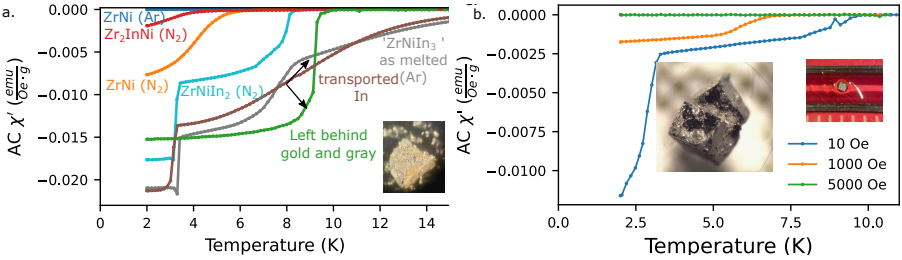

Supplementary Figure 3 The existence of the ∼9 K signal was robust for both arc melted samples and "single crystals". To rule out ZrN impurities as the source of the superconducting signal, we arc melted samples of ZrNi and Zr_2NiIn, and $ZrNiIn_2$ stoichiometry under nitrogen (a). ZrN was identified using XRD in these samples. When ZrNi was melted under argon like most of our samples containing the ∼9 K signal, no superconducting transition was observed. The ∼9 K signal was only visible in samples with indium-rich compositions. Indium acted as a useful internal standard such that the strength of its superconducting signal could be compared to the strength of the ∼9 K signal to determine the relative fraction of sample that superconducts at different temperatures. The strength of the indium signal is relatively comparable to the strength of the ∼9 K signal (when indium could be clearly observed using XRD), indicating that the ∼9 K transition is a bulk behavior. Furthermore, when indium was vapor transported away from the bulk of an indium-rich sample arc melted under argon, the leftover bulk of material exhibited a strong superconducting signal without indium. A photo of this material is shown in (a). Single crystals of In_5Ni_3 grown in an indium flux (b) contained varying amounts of the ∼9 K superconducting phase, demonstrating that some amount of the ∼9 K superconductor forms in materials made using vastly different growth techniques, suggestive of the metaphase nature of the actual superconductor in this phase diagram. As the magnetic field increased, the ∼9 K signal shifted to lower temperatures and, by 5000 Oe, disappeared. This is further evidence that the ∼9 K transition is a bulk behavior.

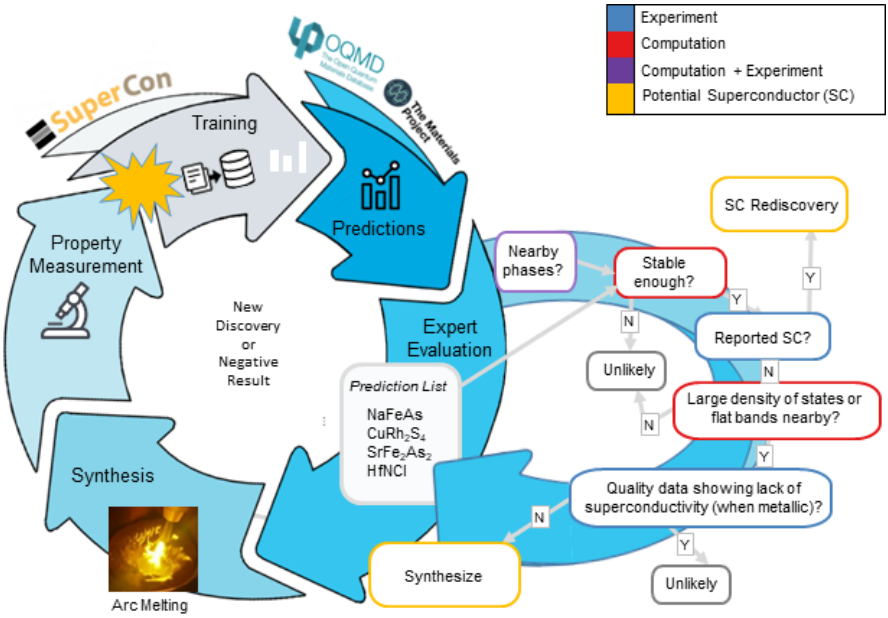

Supplementary Figure 4 machine learning (ML) Prediction-expert evaluation-experimental measurement loop and expert evaluation process. We closed the ML prediction-experimental measurement loop four times in this study. To improve success, experts evaluated lists of predicted superconductors following the procedure outlined to the right to determine which predictions were most promising. When evaluating these predictions, the data sources referenced are denoted by color. "Experiment" includes both literature data and internal data collected in prior loop iterations. "Computation" includes data from computational databases, computed literature data, and targeted computational data that we acquired.

References

[1] Goodall, R.E.A., Lee, A.A.: Predicting materials properties without crystal structure: deep representation learning from stoichiometry. Nat. Comm. 2020 11:1 **11**, 1–9 (2020). https://doi.org/10.1038/s41467-020-19964-7

[2] Zaremba, V., Kaczorowski, D., Gulaj, L.D.: Crystal structure, magnetic and electrical properties of $ZrNi_2In$ and $ZrCu_2In$. J. Alloys Compd. **292**, 1–3 (1999)

[3] Zaleski, A.J., Kaczorowski, D., Zaremba, V.I.: $ZrNi_2In$ - New Superconducting Heusler Alloy. In: E-MRS Fall Meeting, Symposium E Poster, pp. 152–152. E-MRS, Warsaw, Poland (2004). http://science24.com/paper/2054

[4] Winterlik, J., Fecher, G.H., Felser, C., Jourdan, M., Grube, K., Hardy, F., Von Löhneysen, H., Holman, K.L., Cava, R.J.: Ni-based superconductor: Heusler compound $ZrNi_2Ga$. Phys. Rev. B - Condensed Matter and Materials Physics **78**(18), 1–9 (2008). https://doi.org/10.1103/PhysRevB.78.184506

[5] Wernick, J.H., Hull, G.W., Geballe, T.H., Bernardini, J.E., Waszczak, J.V.: Superconductivity in ternary Heusler intermetallic compounds. Mater. Lett. **2**(2), 90–92 (1983). https://doi.org/10.1016/0167-577X(83)90043-5

[6] Jain, A., Ong, S.P., Hautier, G., Chen, W., Richards, W.D., Dacek, S., Cholia, S., Gunter, D., Skinner, D., Ceder, G., Persson, K.A.: Commentary: The materials project: A materials genome approach to accelerating

materials innovation. APL Mater. **1**, 011002 (2013). https://doi.org/10.1063/1.4812323

[7] Lengauer, W.: Characterization of nitrogen distribution profiles in fcc transition metal nitrides by means of Tc measurements. Surface and Interface Analysis **15**(6), 377–382 (1990). https://doi.org/10.1002/sia.740150606